J Intell Robot Syst (2015) 77:113–133
DOI 10.1007/s10846-014-0094-x

# Relative Localization Approach for Combined Aerial and Ground Robotic System

**Thumeera R. Wanasinghe · George K. I. Mann · Raymond G. Gosine**

Received: 27 January 2014 / Accepted: 8 August 2014 / Published online: 27 August 2014


**Abstract** The objective of this paper is to develop a relative localization method for coordinated control of multi-robotic systems equipped with both aerial and ground vehicles. To overcome the issues of filter initialization and state bias at hard linearization in the general EKF approach, this paper proposes a pseudo-linear measurement-based technique for relative localization where true nonlinear measurements are algebraically transformed into pseudo-linear measurements. These pseudo-linear measurements are then employed for sensor fusion. A nonlinear observability analysis is performed to identify the sufficient conditions under which the proposed pseudo-linear measurement-based relative localization scheme is locally weakly observable. The estimation consistency is analyzed in order to verify that the proposed estimator is consistent and that none of the covariance matrixes lead to ill conditions during the estimation process. The performance of the proposed relative localization scheme is compared with traditional EKF-based methods for unknown filter initialization. The results demonstrate that the proposed method is capable of achieving both the acceptable positional and orientational accuracy within 12 iterations, whereas traditional methods require more than 250 iterations to achieve the same accuracy. This observation verified that the proposed relative localization approach has fast convergence property for unknown filter initialization compared to traditional EKF-based methods.

**Keywords** Multi-robotic system · Relative localization · Pseudo-linear measurements · Nonlinear observability · Aerial and ground vehicles.

T. R. Wanasinghe (✉) · G. K. I. Mann · R. G. Gosine
IS Lab, Faculty of Engineering and Applied Science
Memorial, University of Newfoundland, St. John's,
NL A1B 3X5 Canada
e-mail: thumeerawa@mun.ca

G. K. I. Mann
e-mail: gmann@mun.ca

R. G. Gosine
e-mail: rgosine@mun.ca

## 1 Introduction

Multi-robotic systems (MRS) have been receiving attention from the autonomous robotic community due to their distinct advantages over single-robot systems. Robustness to individual failure, better area coverage, and in some cases shorter mission completion times are some of the benefits that MRS can offer. A heterogeneous robotic system with both aerial and ground robots can enhance the capabilities in a 3D sense and improve accessibility. For example, a micro-aerial vehicle (MAV) can manoeuvre in cluttered indoor environments and explore indoor multi-storied buildings in places where navigation of ground robots is difficult.

Estimation of relative positions within an MRS is important for many collective operations. Some

examples are inter-robot collision avoidance [1], pattern generation [2–4], self-configuration [5], flocking [6–8], and chain formation [9]. In the absence of a common global frame of reference and associated inter-robot pose estimates, MRS encounter difficulty in performing effective coordination and collaborative mission executions. As a result, relative localization (RL) has been developed as a viable solution for effective and accurate execution of multi-robot collaborative missions where robots mutually track neighbours in their individual body-fixed coordinate frames [10, 11]. Moreover, RL has been identified as a feasible method of establishing the localization for less capable robots in a heterogeneous MRS. In [12, 13], a leader robot with higher processing and sensing capabilities is utilized to establish accurate inter-robot localization of a much less powerful group of robots operating in a coordinated mission.

The range and bearing[1] between a pair of robots are commonly considered the most important measurements required for establishing the inter-robot relative observation, and the extended Kalman filter (EKF) has been the widely applied sub-optimal nonlinear estimator for realizing the RL [13–15]. Poor initialization of EKF generally causes instability [13], leading to failure in the gating validation and causing for singularity in the innovation covariances. Additionally, unknown initialization causes a wider settling time[2] in tracking and this in turn results in erroneous interpretation of one robot's observation in another robot's body-fixed coordinate frame. This erroneous interpretation can lead to unpredictable behaviour and failure in collaborative missions. This issue is traditionally resolved by assuming a known transformation between two given robots at the initial encounter [16, 17].

Our early study exploited a pseudo-linear measurement-based estimation approach for RL [18] as an alternative to the traditional EKF-based approaches. It surfaced that the pseudo-linear measurement based RL scheme possesses a fast convergence property compared to its EKF-based counterpart. This paper is the extended version of [18] and makes the following contributions: 1) A stable and faster convergence filtering solution for RL; the proposed system converges within 12 iterations, whereas the traditional approaches take more than 250 iterations before reaching an acceptable accuracy level for inaccurate filter initialization. Moreover, in the proposed method the initial position can be assumed to be arbitrary within the sensing range of the tracking robot. 2) Nonlinear observability analysis for pseudo-linear measurement-based RL schemes; the conversion of the nonlinear inter-robot relative measurements into a pseudo-linear format affects the system observability conditions. We performed Lie derivatives-based nonlinear observability analysis for the proposed RL scheme and derived sufficient conditions for the system to be locally weakly observable for different relative measurement combinations. 3) Consistency analysis for pseudo-linear measurement-based RL schemes; as measurements are transformed into a pseudo-linear format the corresponding measurement variances become a function of estimated states. The measurement error covariance $\mathbf{R}$ then becomes a time dependent compared to the constant measurement covariance in traditional EKF approaches. Our consistency analysis showed that this time dependant nature of $\mathbf{R}$ does not lead to inconsistent state estimation.

This paper is organized as follows. Overview of the multi-robot localization and system observability analysis are presented in Section 2. Section 3 describes the proposed pseudo-linear measurement based RL scheme. Section 4 presents sufficient conditions that system needs to be satisfied in order to guarantee for full system observability when a RL scheme is implemented using pseudo-linear relative measurements. Simulation setup and results are described in Section 5. Experimental validation is presented in Section 6. Section 7 presents the results of the consistency analysis. Finally, Section 8 derives the conclusions, states the limitations, and projects the potential extensions for the proposed method.

## 2 Background

Localization methods available for mobile agents can be categorized into two major groups: absolute localization and RL. In the absolute localization approach, the robots are empowered with absolute positioning capabilities. The most direct method is the use of global positioning system (GPS) or differential GPS sensors where the accuracy is limited to the GPS accuracies found in the commercial sensor. The other

[1] Both azimuth and elevation angles.

[2] Time taken to reach acceptable error level.

popular indirect measurement methods include simultaneous localization and mapping (SLAM) [19] using a common reference frame defined at the very beginning of the mission, and cooperative localization [20, 21] where through sharing sensor information and inter-robot observations, members in an MRS refine their pose with respect to a common reference frame. In contrast to the absolute localization methods, in the RL a robot tracks its neighbours with respect to a body-fixed coordinate system on the robot using inter-robot relative measurements [10–13], typically the range and bearing information.

Most relative observation based approaches employ filter based solutions or geometry/model based solutions for localization. The common filters have been the extended Kalman filter (EKF)[13–15], particle filter [19] and unscented Kalman filter (UKF) [22]. The geometry/model based approaches compute inter-robot transformation using relative measurements and the pose of the observed robot. Recently, a pseudo-linear Kalman filter was applied to solve a SLAM problem [23, 24] where nonlinear relative measurements have been algebraically transformed into the linear format for sensor fusion. This pseudo-linear based approach originated in [25] and introduced in order to overcome instability and bias problems associated with the measurement linearization in EKF.

Vision and acoustic based approaches are reported for inter-robot relative measurements [26–29]. Vision only solutions [26, 27] generally demand higher computational power in order to extract the depth information, while acoustic only solutions [28, 29] require an array of acoustic sensors to establish a reasonably accurate bearing estimate. The study in [13] combines the complimentary unique characteristics of vision and acoustic based approaches and presents a relative observation framework. In addition to vision and acoustic solutions, laser range finders are also employed for relative range and bearing measurements [21]. Franchi et al. [30] used laser range finders based approach and extended general relative observation scenarios into anonymous mutual observation scenarios for RL estimates. In [31] a stationary synchronized sensor network has been installed in the robot environment to receive relative observations of multiple robots. However, applicability of this method is limited to known, well-structured environments as they require pre-installation of infrastructure.

It is known that both the qualitative and quantitative performances of any estimator depend on system observability. The rank of Gramian matrix [32] and the Popov-Belevitch-Hautus (PBH) test [33] were developed to evaluate the system observability for linear time-invariant systems. Graph-based observability analysis using the Lie derivatives [34, 35], and observability rank condition tests based on the Lie derivatives [36–39], were reported for nonlinear observability analysis. These nonlinear observability analysis techniques capture the nonlinearity of the dynamics and observation. Additionally, control signals were also considered in these nonlinear observability analysis techniques, which are not considered in linear observability analysis. [36] has presented complete nonlinear observability analysis for inter-robot 3D transformation; however, this analysis considers true nonlinear measurements and their equivalent linear formats for the nonlinear observability analysis. [37] presents nonlinear observability analysis in a polar-Cartesian mixed coordinate system. How the system observability is affected by the transformation of nonlinear measurements into pseudo-linear formats has not been studied yet. Our study fills this gap by presenting Lie derivative-based nonlinear observability analysis for pseudo-linear measurement-based RL schemes.

## 3 Problem Formulation

In this section, relative localization for air-ground MRS is formulated, the construction of pseudo-linear observer from inter-robot relative observation is introduced, and simplified measurement covariance matrix for pseudo-linear observer is presented.

In order to improve the clarity of the presentation, two terms that widely used in this paper are introduced below:

**Observing Robot**: A robot taking range and bearing measurement for an arbitrary robot in its fields of view is termed as an *observing robot*. The superscript or subscript $l$ is used to represent variables that are related to an observing robot.

**Observed Robot**: A robot who is under gone measurements by an observing robot is termed as an *observed robot*. The superscript or subscript $c$ is used to represent variables that are related to an observed robot.

Therefore, the objective is to establish the RL of the observed robots in the body-fixed coordinate system of the observing robot using inter-robot relative measurements between them.

### 3.1 Problem Statement

Assume at any time instant $k$, a team of robots contains $N$ observed robots ($\mathcal{R}_{c1}, \mathcal{R}_{c2}, \mathcal{R}_{c3}, ..., \mathcal{R}_{cN}$) and $M$ observing robots ($\mathcal{R}_{l1}, \mathcal{R}_{l2}, \mathcal{R}_{l3}, ..., \mathcal{R}_{lM}$), where $N \in \mathbb{Z}^+$ and $M \in \mathbb{Z}^+$ and are unknown to each robot and also may vary with the time. The navigational space is assumed to be three-dimensional and bounded. The relative pose of the $i^{th}$ observed robot in $j^{th}$ observing robot's local Cartesian coordinate frame at any time step $k$ is given by the position $(x, y, z)^{lj}_{ci,k}$ and the orientation $(\phi)^{lj}_{ci,k}$.[3] For the proposed system, the robots in the MRS should have the following characteristics:

1. Each robot platform in the MRS has dead-reckoning capability.
2. A robot that qualifies to be an observing robot is equipped with exteroceptive sensors in order to uniquely identify each of the observed robots in its field of view.
3. An observing robot has the ability to measure range and bearing of all other observed robots with respect to its body-fixed coordinated frame.
4. Aerial robots can only be in the observed robot category, and we assume aerial robots do not have sufficient sensing and processing capabilities to be in the class of observing robots.
5. Each robot platform contains a communication device to exchange information between all other robots.
6. The operational environment is such that the ground robots navigate in flat surfaces and the aerial robots obey the hovering conditions. Hovering condition is a valid assumption for micro-aerial vehicles (MAVs) as they possess a sufficiently accurate low-level controller loop to stabilize the pitch and roll angles at low velocity maneuvers.

[3] Note that, hereafter equations are presented for a single observing robot and a single observed robot. Thus, superscript $lj$ and subscript $ci$ may omitted from some equations. Additionally, time symbol $k$ will also be omitted for the simplicity of the presentation.

A sample robot configuration of the proposed relative localization scheme for a given time instance $k$ is illustrated in Fig. 1.

Label $R_{lm}$ ($m \in \{1, 2\}$) represents robots with exteroceptive sensing capabilities while label $R_{cn}$ ($n \in \{1, 2, 3, 4, 5, 6\}$) represents those without exteroceptive sensing capabilities. $R_{c1}$, $R_{c3}$ and $R_{c6}$ are aerial observed robots and $R_{c2}$, $R_{c4}$ and $R_{c5}$ are ground observed robots. ${}^{j}(r, \theta, \alpha)_i$ is relative range, relative azimuth angle and relative elevation angle of robot $i$ measured by robot $j$. Note that at this time instance, $R_{l2}$ operates as an observing robot for $R_{c3}$, $R_{c5}$, and $R_{c6}$ and acts as an observed robot for $R_{l1}$ simultaneously.

### 3.2 Relative State Propagation Model

A robot navigating in three-dimensional space is generally described in a six degree of freedom (DOF) kinematic model [36]. The sixth characteristic that we have assumed in this research (Section 3.1) allows for a simplification of the 6-DOF kinematic model into a 4-DOF model. The modified relative state propagation model is given in Eq. 2.

$$\dot{\mathbf{x}} = \mathbf{f}(\mathbf{x}, \mathbf{u}_l, \mathbf{u}_c) + \nu_{\mathbf{x}} \tag{1}$$

$$\begin{bmatrix} \dot{x} \\ \dot{y} \\ \dot{z} \\ \dot{\phi} \end{bmatrix} = \begin{bmatrix} u_{x,c}\cos\phi - u_{y,c}\sin\phi - u_{x,l} + y\omega_{z,l} \\ u_{y,c}\cos\phi + u_{x,c}\sin\phi - u_{y,l} - x\omega_{z,l} \\ u_{z,c} - u_{z,l} \\ \omega_{z,l} - \omega_{z,l} \end{bmatrix} + \nu_{\mathbf{x}}$$

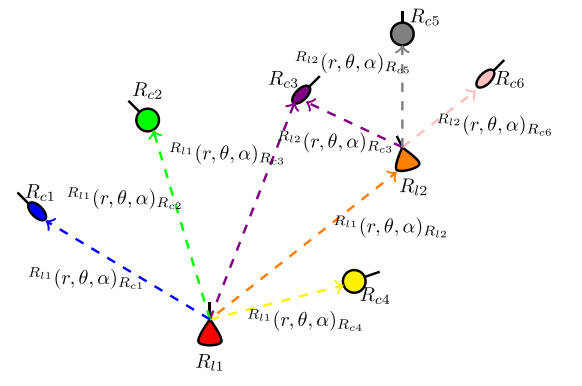


**Fig. 1** Sample robot configuration at a given time instance $k$

where, $\mathbf{x} \in \mathbb{R}^n$ is the relative state vector, i.e. $\mathbf{x} = [x\ y\ z\ \phi]^T$ where, $x$, $y$ and $z$ gives relative position and $\phi$ is relative orientation of an observed robot in an observing robot body-fixed coordinate system; $\mathbf{u}_l \in \mathbb{R}^{nl}$ is control input vector of the observing robot, in other words body-fixed velocities of the observing robot, i.e. $\mathbf{u}_l = \begin{bmatrix} u_{x,l}\ u_{y,l}\ u_{z,l}\ \omega_{z,l} \end{bmatrix}^T$ where, $u_{x,l}$, $u_{y,l}$, $u_{z,l}$ and $\omega_{z,l}$ represent linear and angular body-fixed velocities of an observing robot; $\mathbf{u}_c \in \mathbb{R}^{nc}$ is control input vector of the observed robot, i.e. $\mathbf{u}_c = \begin{bmatrix} u_{x,c}\ u_{y,c}\ u_{z,c}\ \omega_{z,c} \end{bmatrix}^T$ where, $u_{x,c}$, $u_{y,c}$, $u_{z,c}$ and $\omega_{z,c}$ represent linear and angular body-fixed velocities of an observed robot; and $\nu_{\mathbf{x}}$ is zero mean, additive white Gaussian noise term that accounts unmodelled system dynamics and system modeling inaccuracies. For the modified relative state propagation model, dimensional variables $n$, $nl$ and $nc$ are equal to four (i.e. $n = nl = nc = 4$).

### 3.3 Inter-robot Observation Model

In the proposed method, it is assumed that the observing robots are equipped with exteroceptive sensors which provide 3D ranging and bearing for observed robots. Furthermore, it is assumed that local coordinate frame of sensor nodes coincide with the robots' body-fixed coordinate frame. The inter-robot observation model is then given in Eq. 3.

$$\mathbf{y}_{pco} = \mathbf{g}(\mathbf{x}) + \nu_{pco} \tag{2}$$

$$\begin{bmatrix} r \\ \theta \\ \alpha \end{bmatrix} = \begin{bmatrix} \sqrt{x^2+y^2+z^2} \\ \arctan\left(\frac{y}{x}\right) \\ \arctan\left(\frac{z}{\sqrt{x^2+y^2}}\right) \end{bmatrix} + \begin{bmatrix} \nu_r \\ \nu_\theta \\ \nu_\alpha \end{bmatrix}$$

where, $r$, $\theta$ and $\alpha$ are relative range, relative azimuth angle, and relative elevation angle, respectively. $x$, $y$ and $z$ are relative positions of an observed robot. Parameters $\nu_r$, $\nu_\theta$ and $\nu_\alpha$ are zero mean, additive white Gaussian noise terms for measurements and are defined as follows:

$$\nu_r \sim \mathcal{N}(0, \sigma_r^2) \nu_\theta \sim \mathcal{N}(0, \sigma_\theta^2) \nu_\alpha \sim \mathcal{N}(0, \sigma_\alpha^2).$$

Traditional EKF approaches directly linearize this nonlinear measurements model, and linearized measurements are applied for sensor fusion. Explicit linearization of measurement introduces a bias problem and loss of information [23, 40]. To overcome these issues, in this study, nonlinear observations are algebraically transformed and constructed a new series of relative measurements, called pseudo-linear measurements [41]. The inter-robot observation model is then defined by $\bar{\mathbf{g}}(\mathbf{x})$ and is given in Eq. 3.

$$\mathbf{y}_{pmo} = \bar{\mathbf{g}}(\mathbf{x}) = \mathbf{H}_{pmo}\mathbf{x} + \nu_{pm}(\mathbf{x}, \nu_{\mathbf{x}}) \tag{3}$$

$$\begin{bmatrix} y_1 \\ y_2 \\ y_3 \end{bmatrix} \triangleq \begin{bmatrix} r \\ 0 \\ 0 \end{bmatrix} = \begin{bmatrix} c\theta c\alpha & s\theta c\alpha & s\alpha & 0 \\ -s\theta & c\theta & 0 & 0 \\ -c\theta s\alpha & -s\theta s\alpha & c\alpha & 0 \end{bmatrix} \mathbf{x} + \nu_{pm}(\mathbf{x}, \nu_{\mathbf{x}})$$

where $c\theta = \cos\theta, c\alpha = \cos\alpha, s\theta = \sin\theta, s\alpha = \sin\alpha$. $r$ is true relative range measurement. Note that the first pseudo-linear measurement, $y_1$, is equivalent to the noisy relative range measurement, $r$, while the second and the third pseudo-linear measurements, $y_2$ and $y_3$, are equivalent to zero. Therefore, $\begin{bmatrix} r\ 0\ 0 \end{bmatrix}^T$ is used as the measured pseudo-linear values at the measurement update step of the Kalman filter while the corresponding predicted pseudo-linear measurement values are obtained using the measurement model given in Eq. 3, and the noisy bearing measurements $\theta$ and $\alpha$. Resulting pseudo-linear measurements ($y_1$, $y_2$, $y_3$) are linear with respect to system states, and also their measurement coefficient matrix, $\mathbf{H}_{pmo}$, becomes a nonlinear function of true measurements ($r$, $\theta$, $\alpha$).

Covariance of the pseudo-linear measurement , i.e. $\mathbf{R}_{pmo}$, is derived from Eq. 4.

$$\mathbf{R}_{pmo} = \mathbf{J}^T \begin{bmatrix} \sigma_r^2 & 0 & 0 \\ 0 & \sigma_\theta^2 & 0 \\ 0 & 0 & \sigma_\alpha^2 \end{bmatrix} \mathbf{J} \tag{4}$$

where, $J$ is the Jacobian of the pseudo-linear measurement in Eq. 4 with respect to true measurements $r$, $\theta$, and $\alpha$, i.e

$$\mathbf{J} = \left.\frac{\partial(\mathbf{y}_{pmo})}{\partial(r,\theta,\alpha)}\right|_{r=\bar{r},\ \theta=\bar{\theta},\ \alpha=\bar{\alpha}} \tag{5}$$

where $\bar{r}$, $\bar{\theta}$, and $\bar{\alpha}$ are noisy relative measurements for an observed robot. The state dependent pseudo-linear noise covariance matrix can be simplified to derive a temporally uncorrelated pseudo-linear measurement no- ise covariance matrix and is given in Eq. 6 [42].

$$\mathbf{R}_{pmo} = \begin{bmatrix} \sigma_r^2 & 0 & 0 \\ 0 & (x^2+y^2)\sigma_\theta^2 & 0 \\ 0 & 0 & (x^2+y^2+z^2)\sigma_\alpha^2 \end{bmatrix} \tag{6}$$

Note that the true states are not available and estimated states are utilized to calculate the measurement

covariance matrix. Furthermore, it can be seen that pseudo-linear measurement errors are state dependent.

### 3.4 Sensor Fusion

The EKF is employed for sensor fusion. Prediction and correction structures of EKF are summarized in Eqs. 8 and 9, respectively. Note that the proposed pseudo-linear measurements are used at the correction step of the sensor fusion instead of nonlinear range and bearing measurements.

Prediction

$$\begin{aligned} \dot{\hat{\mathbf{x}}}^{-} &= \mathbf{f}(\hat{\mathbf{x}}, \mathbf{u}_l, \mathbf{u}_c) \\ \mathbf{F} &= \tfrac{\partial}{\partial \mathbf{x}} \mathbf{f}(\hat{\mathbf{x}}, \mathbf{u}_l, \mathbf{u}_c) \big|_{\mathbf{x}=\hat{\mathbf{x}}} \\ \mathbf{P}^{-} &= \mathbf{F}\mathbf{P}\mathbf{F}^{T} + \mathbf{Q} \end{aligned} \tag{7}$$

Correction

$$\begin{aligned} \hat{\mathbf{y}} &= \bar{\mathbf{g}}(\hat{\mathbf{x}}) \\ \mathbf{K} &= \mathbf{P}\mathbf{H}_{\mathbf{pmo}}^{\mathbf{T}}(\mathbf{H}_{\mathbf{pmo}}\mathbf{P}\mathbf{H}_{\mathbf{pmo}}^{\mathbf{T}} + \mathbf{R}_{\mathbf{pmo}})^{-1} \\ \hat{\mathbf{x}}^{+} &= \hat{\mathbf{x}}^{-} + \mathbf{K}(\mathbf{z} - \hat{\mathbf{y}}) \\ \mathbf{P} &= \mathbf{P}^{-} - \mathbf{K}\mathbf{H}_{\mathbf{pmo}}\mathbf{P}^{-} \end{aligned} \tag{8}$$

$\hat{\mathbf{y}}$ represents the predicted pseudo-linear measurements using noisy bearing measurements as given in Eq. 3. Measurement matrix $\mathbf{H}_{pmo}$ is constructed as shown in Eq. 3, and the corresponding measurement covariance $\mathbf{R}_{pmo}$ is realized from Eq. 6. $\mathbf{z}$ is the noisy pseudo-linear measurement vector and is given by $[r\ 0\ 0]^T$; where, $r$ is noisy range measurement.

## 4 Observability Analysis

The conversion of the nonlinear inter-robot relative measurements into the pseudo-linear format may affect the system observability. Hence, it is essential to investigate the system observability for pseudo-linear relative measurements. Note that the 4-DOF relative motion model given in Eq. 2 is nonlinear although the inter-robot observation model given in Eq. 3 are linear with respect to the state variables. Thus, the rank of Gramian matrix [32] or the Popov-Belevitch-Hautus test [33] are not applicable methods to evaluate the system observability as they are designed for linear time-invariant systems. Graph-based nonlinear observability analysis is introduced recently and applied to evaluate the observability of the bearing only cooperative localization [34, 35] while the observability rank condition test based on the Lie derivatives [36–39] is well established and widely employed method for nonlinear observability analysis. Therefore, this study employs the observability rank condition based on the Lie derivatives for the observability analysis of the proposed pseudo-linear measurement-based relative localization scheme. Although we exploit both relative range and relative bearing capabilities for the proposed relative localization scheme, for the sake of completeness, following observability study is presented for leader-based range and bearing measurement system, leader-based relative bearing only measurement system, and leader-based relative range only measurement system.

### 4.1 Nonlinear Observability

For a nonlinear system, local observability is more sought as the global observability is typically difficult to achieve [38]. For a given continuous-time nonlinear system as described in Eq. 9, corresponding control affine form can be written as Eq. 10.

$$\begin{cases} \dot{\mathbf{x}} = \mathbf{f}(\mathbf{x}, \mathbf{u}) \\ \mathbf{y} = \mathbf{h}(\mathbf{x}) \end{cases} \tag{9}$$

$$\begin{cases} \dot{\mathbf{x}} = \mathbf{f}_{\circ}(\mathbf{x}) + \sum\limits_{\forall i=1:q} \mathbf{f}_i(\mathbf{x}) u_i \\ \mathbf{y} = \mathbf{h}(\mathbf{x}) \end{cases} \tag{10}$$

where, $\mathbf{x} \in \mathbb{R}^n$ is the state vector, $\mathbf{u} = [u_1 \cdots u_q]^T \in \mathbb{R}^q$ is the control input vector, $\mathbf{y} = [y_1 \cdots y_m]^T \in \mathbb{R}^m$ is the measurement vector and $\mathbf{f}_{\circ}(\mathbf{x})$ characterizes system dynamics at zero input conditions. $\mathbf{f}_i(\mathbf{x})$ characterizes system dynamics for the $i^{th}$ input, i.e. $u_i$, and can be given as $\mathbf{f}_i(\mathbf{x}) = [f_{i1}(\mathbf{x})\ \ f_{i2}(\mathbf{x})\ \ \cdots\ \ f_{in}(\mathbf{x})]^T$. The observability matrix is then defined as the matrix of zero-order through $(n-1)$ order of Lie-derivatives. In other word, a matrix with rows as given in Eq. 11 is defined as the observability matrix.

$$\begin{aligned} \mathcal{O} \triangleq \{ \nabla \mathfrak{L}^{q}_{f_i \cdots f_j} h_p(\mathbf{x}) | \quad & i, j = 0, \cdots, q; \\ & p = 1, \cdots, m; q \in \mathbb{N} \} \end{aligned} \tag{11}$$

where, $\mathfrak{L}$ represents the Lie-derivative, $q$ represents the order of the Lie-derivative, $\nabla$ represents the gradient operator. Measurement model may consists of $m$

number of measurements. An introduction to the Lie-deriva- tives can be found in [36, VII-A.]. Definition 1 and Theorem 1 which are adopted from [39, Th. 3.1] employ to evaluate the observability of a nonlinear system.

**Definition 1** A nonlinear system is satisfied the *observability rank condition* when the observability matrix defined in Eq. 11 is full rank.

**Theorem 1** *If a nonlinear system satisfies the observability rank condition then the nonlinear system is locally weakly observable. This is known as sufficient condition for the observability.*

### 4.2 Continuous-Time Relative Motion Model

The control affine form of the continuous-time relative state propagation model is given in Eq. 1 can be written as follows:

$$\underbrace{\begin{bmatrix}\dot{\mathbf{p}}\\ \dot{\phi}\end{bmatrix}}_{\dot{\mathbf{x}}_c^l} = \underbrace{\begin{bmatrix}-\mathbf{I}_3\\ \mathbf{0}_{1\times 3}\end{bmatrix}}_{f_1}\mathbf{v}_l + \underbrace{\begin{bmatrix}\mathbf{C}\\ \mathbf{0}_{1\times 3}\end{bmatrix}}_{f_2}\mathbf{v}_c + \underbrace{\begin{bmatrix}\lfloor \mathbf{p}\times [0\ 0\ 1]^T \rfloor\\ -1\end{bmatrix}}_{f_3}\omega_{z,l} + \underbrace{\begin{bmatrix}\mathbf{0}_{3\times 1}\\ 1\end{bmatrix}}_{f_4}\omega_{z,c} \tag{12}$$

where, $\mathbf{I}_3$ is $3 \times 3$ identity matrix, $\mathbf{C}$ is the rotational matrix around $z$-axis which is given in Eq. 13, $\mathbf{p}$ is the relative position vector, and $\mathbf{v}_l$ and $\mathbf{v}_c$ are the body-fixed linear velocities of observing robot and observed robot, respectively, $\mathbf{v}_l = [u_{x,l}\ u_{y,l}\ u_{z,l}]^T$ and $\mathbf{v}_c = [u_{x,c}\ u_{y,c}\ u_{z,c}]^T$, and $\omega_{z,l}$ and $\omega_{z,c}$ are the body-fixed yaw rate of observing and observed robot, respectively.

$$\mathbf{C} = \begin{bmatrix}\cos(\phi) & -\sin(\phi) & 0\\ \sin(\phi) & \cos(\phi) & 0\\ 0 & 0 & 1\end{bmatrix} \tag{13}$$

### 4.3 Observability of the Relative Localization for Different Relative Measurement Combinations

**Case 1**: Range and bearing measurements are available

When an exteroceptive sensory system is capable of measuring 3D range and bearing for an observed robot, then the corresponding pseudo-linear measurement model is illustrated in Eq. 3. The pseudo-linear relative measurement function, $\mathbf{h}(\mathbf{x})$, can then be expressed as below:

$$\mathbf{h}(\mathbf{x}) = \begin{bmatrix} xc(\theta)c(\alpha) + ys(\theta)c(\alpha) + zs(\alpha)\\ -xs(\theta) + yc(\theta)\\ -xc(\theta)s(\alpha) - ys(\theta)s(\alpha) + zc(\alpha)\end{bmatrix} \tag{14}$$

– Zeroth-order Lie derivatives ($\mathfrak{L}^{\circ}\mathbf{h}$)

The function itself becomes the zeroth-order Lie derivative of a function [36].

$$\mathfrak{L}^{\circ}\mathbf{h} = \mathbf{h}(\mathbf{x}) \tag{15}$$

The gradient of the Eq. 15 is as follows:

$$\nabla\mathfrak{L}^{\circ}\mathbf{h} = \begin{bmatrix} c(\theta)c(\alpha) & s(\theta)s(\alpha) & s(\alpha) & 0\\ -s(\theta) & c(\theta) & 0 & 0\\ -c(\theta)s(\alpha) & -s(\theta)s(\alpha) & c(\alpha) & 0\end{bmatrix} = \begin{bmatrix}\mathbf{h}_{pmo} & 0_{3\times 1}\end{bmatrix} \tag{16}$$

– First-order Lie derivatives ($\mathfrak{L}^1_{\mathbf{f}_2}\mathbf{h}$)

$$\mathfrak{L}^1_{\mathbf{f}_2}\mathbf{h} = \nabla\mathfrak{L}^{\circ}\mathbf{y}.f_2 = \begin{bmatrix}\mathbf{h}_{pmo} & 0_{3\times 1}\end{bmatrix}.\begin{bmatrix}\mathbf{C}\\ 0_{1\times 3}\end{bmatrix} = \mathbf{h}_{pmo}.\mathbf{C} \tag{17}$$

This contains only relative orientation components. Hence, take gradient of $\mathfrak{L}^1_{\mathbf{f}_2}\mathbf{h}$ with respect to $\phi$. Note that column of Eq. 17 are stacked to form a $9\times 1$ vector prior to compute the gradient of $\mathfrak{L}^1_{\mathbf{f}_2}\mathbf{h}$ with respect to $\phi$.

$$\nabla_{\phi}\mathfrak{L}^1_{\mathbf{f}_2}\mathbf{h} = \begin{bmatrix} c(\phi)s(\alpha)s(\theta) - s(\phi)c(\alpha)c(\theta)\\ c(\phi)c(\theta) + s(\phi)s(\theta)\\ s(\phi)s(\alpha)c(\theta) - c(\phi)s(\alpha)s(\theta)\\ -c(\phi)c(\alpha)c(\theta) - s(\phi)s(\alpha)s(\theta)\\ c(\phi)s(\theta) - s(\phi)c(\theta)\\ c(\phi)s(\alpha)c(\theta) + s(\phi)s(\alpha)s(\theta)\\ 0\\ 0\\ 0\end{bmatrix} \tag{18}$$

**Lemma 1** *Given the 3D range and bearing measurements, a sufficient condition for the system given in* Eqs. 12 *and* 14 *to be locally weakly observable is* $\mathbf{v}_c \neq 0$

*Proof* Given the 3D range and bearing measurements, the observability matrix for the system

expressed in Eqs. 12 and 14 can be constructed using Eqs. 16 and 18 and is given as follows:

$$\mathcal{O}_1 = \begin{bmatrix} \nabla \mathfrak{L}^{\circ} \mathbf{h} \\ \nabla \mathfrak{L}^{1}_{\mathbf{f}_2} \mathbf{h} \end{bmatrix} = \begin{bmatrix} \mathbf{h}_{pmo} & 0_{3\times 1} \\ 0_{9\times 3} & \nabla_{\phi} \mathfrak{L}^{1}_{\mathbf{f}_2} \mathbf{h} \end{bmatrix} \tag{19}$$

It is sufficient to show that the $\mathbf{h}_{pmo}$ and $\nabla_{\phi} \mathfrak{L}^{1}_{\mathbf{f}_2} \mathbf{h}$ are full rank in order to prove that the $\mathcal{O}_1$ retains full column rank condition.

$$\begin{aligned} \det(\mathbf{h}_{pmo}) \;=\; & c(\alpha)^2 c(\theta)^2 + c(\alpha) s(\alpha) s(\theta)^2 \\ & + s(\alpha)^2 c(\theta)^2 + s(\alpha)^2 s(\theta^2) \neq 0 \end{aligned} \tag{20}$$

$$\begin{aligned} \det\left( (\nabla_{\phi} \mathfrak{L}^{1}_{\mathbf{f}_2} \mathbf{h})^T (\nabla_{\phi} \mathfrak{L}^{1}_{\mathbf{f}_2} \mathbf{h}) \right) \;=\; & 2 s(\alpha)^2 s(\theta)^2 \\ & - s(\theta)^2 + 2 \neq 0 \end{aligned} \tag{21}$$

According to Eqs. 20 and 21, $\mathbf{h}_{pmo}$ and $\nabla_{\phi} \mathfrak{L}^{1}_{\mathbf{f}_2} \mathbf{h}$ are full rank. Hence, $\mathcal{O}_1$ has full column rank; thus, observability rank condition is satisfied. Therefore, from the Theorem 1, system is locally weakly observable when $\mathbf{v}_c \neq 0$. In other word, pseudo-linear measurement based relative localization scheme that described in Eqs. 12 and 14 is locally weakly observable when an observed robot linear velocities are not equal to zero. □

**Case 2:** Only bearing measurements are available

When system is empowered only with inter-robot relative bearing measurement capabilities, the corresponding pseudo-linear measurement function $\mathbf{h}(\mathbf{x})$ is given in Eq. 22.

$$\mathbf{h}_2(\mathbf{x}) = \begin{bmatrix} -x s(\theta) + y c(\theta) \\ -x c(\theta) s(\alpha) - y s(\theta) s(\alpha) + z c(\alpha) \end{bmatrix} \tag{22}$$

– Zeroth-order Lie derivatives ($\mathfrak{L}^{\circ}\mathbf{h}_2$)

$$\mathfrak{L}^{\circ}\mathbf{h}_2 = \mathbf{h}_2(\mathbf{x}) \tag{23}$$

Its gradient is as follows:

$$\begin{aligned} \nabla \mathfrak{L}^{\circ}\mathbf{h}_2 \;=\; & \begin{bmatrix} -s(\theta) & c(\theta) & 0 & 0 \\ -c(\theta) s(\alpha) & -s(\theta) s(\alpha) & c(\alpha) & 0 \end{bmatrix} \\ =\; & \begin{bmatrix} \mathbf{h}^{\circ}_{pmo_2} & 0_{2\times 1} \end{bmatrix} \end{aligned} \tag{24}$$

– First-order Lie derivatives ($\mathfrak{L}^{1}_{\mathbf{f}_2}\mathbf{h}_2$ and $\mathfrak{L}^{1}_{\mathbf{f}_3}\mathbf{h}_2$)

$$\begin{aligned} \mathfrak{L}^{1}_{f_2}\mathbf{h}_2 \;=\; & \nabla \mathfrak{L}^{\circ}\mathbf{h}_2 \cdot \mathbf{f}_2 \\ =\; & \begin{bmatrix} s(\phi-\theta) & c(\phi-\theta) & 0 \\ -c(\phi-\theta) s(\alpha) & s(\phi-\theta) s(\alpha) & c(\alpha) \end{bmatrix} \end{aligned} \tag{25}$$

This contains only the relative orientation component. Hence, take gradient of $\mathfrak{L}^{1}_{\mathbf{f}_2}\mathbf{h}_2$ with respect to $\phi$.

$$\nabla_{\phi} \mathfrak{L}^{1}_{\mathbf{f}_2} \mathbf{h}_2 = \begin{bmatrix} c(\phi-\theta) \\ s(\phi-\theta) s(\alpha) \\ -s(\phi-\theta) \\ c(\phi-\theta) s(\alpha) \\ 0 \\ 0 \end{bmatrix} \tag{26}$$

$$\begin{aligned} \mathfrak{L}^{1}_{f_3}\mathbf{h}_2 \;=\; & \nabla \mathfrak{L}^{\circ}\mathbf{h}_2 \cdot \mathbf{f}_3 \\ =\; & \begin{bmatrix} -x c(\theta) - y s(\theta) \\ x s(\alpha) s(\theta) - y s(\alpha) c(\theta) \end{bmatrix} \end{aligned} \tag{27}$$

Its gradient is as follows:

$$\begin{aligned} \nabla \mathfrak{L}^{1}_{f_3}\mathbf{h}_2 \;=\; & \begin{bmatrix} -c(\theta) & -s(\theta) & 0 & 0 \\ s(\alpha) s(\theta) & -s(\alpha) c(\theta) & 0 & 0 \end{bmatrix} \\ =\; & \begin{bmatrix} \mathbf{h}^{1}_{pmo_2} & 0_{2\times 1} \end{bmatrix} \end{aligned} \tag{28}$$

**Lemma 2** *Given the 3D bearing measurements, a sufficient condition for the system given in* Eqs. 12 *and* 22 *to be locally weakly observable is 1)* $\mathbf{v}_c \neq 0$ *and 2)* $\omega_{z,l} \neq 0$.

*Proof* Given the 3D bearing measurements, the observability matrix for the system expressed in Eqs. 12 and 22 can be constructed using Eqs. 25, 26 and 28 and is given as follows:

$$\mathcal{O}_2 = \begin{bmatrix} \nabla \mathfrak{L}^{\circ}\mathbf{h}_2 \\ \nabla \mathfrak{L}^{1}_{\mathbf{f}_3}\mathbf{h}_2 \\ \nabla \mathfrak{L}^{1}_{\mathbf{f}_2}\mathbf{h}_2 \end{bmatrix} = \begin{bmatrix} \mathbf{h}^{\circ}_{pmo_2} & 0_{2\times 1} \\ \mathbf{h}^{1}_{pmo_2} & 0_{2\times 1} \\ 0_{6\times 3} & \nabla_{\phi} \mathfrak{L}^{1}_{\mathbf{f}_2}\mathbf{h}_2 \end{bmatrix} \tag{29}$$

It is sufficient to show that both $\begin{bmatrix} \mathbf{h}^{\circ}_{pmo_2} \\ \mathbf{h}^{1}_{pmo_2} \end{bmatrix}$ and $\nabla_{\phi} \mathfrak{L}^{1}_{\mathbf{f}_2}\mathbf{h}_2$ are full rank in order to prove that the $\mathcal{O}_2$ retains full column rank condition.

$$\det\left( \begin{bmatrix} \mathbf{h}^{\circ}_{pmo_2} \\ \mathbf{h}^{1}_{pmo_2} \end{bmatrix}^T \begin{bmatrix} \mathbf{h}^{\circ}_{pmo_2} \\ \mathbf{h}^{1}_{pmo_2} \end{bmatrix} \right) = 1 - s(\alpha)^4 \neq 0 \;\text{ if } \alpha \neq \pm(2n+1)\pi/2n \in \mathbb{Z} \tag{30}$$

$$\det\left( (\nabla_{\phi} \mathfrak{L}^{1}_{\mathbf{f}_2}\mathbf{h}_2)^T (\nabla_{\phi} \mathfrak{L}^{1}_{\mathbf{f}_2}\mathbf{h}_2) \right) = 1 + s(\alpha)^2 \neq 0 \tag{31}$$

According to Eq. 30 and 31, $\begin{matrix} \mathbf{h}^{\circ}_{pmo_2} \\ \mathbf{h}^{1}_{pmo_2} \end{matrix}$ and $\nabla_{\phi} \mathfrak{L}^{1}_{\mathbf{f}_2}\mathbf{h}_2$ are full rank. Hence, $\mathcal{O}_2$ has full column rank; thus, observability rank condition is satisfied. Therefore, from Theorem 1, system is locally weekly observable when 1) $\mathbf{v}_c \neq 0$ and 2) $\omega_{z,l} \neq 0$. In other word, pseudo-linear bearing measurement based relative localization scheme that described in Eqs. 12

and 22 is locally weekly observable when an observed robot linear velocities and an observing robot angular velocities are not equal to zero. □

It is important to note that $\mathbf{v}_c \neq 0$ and $\mathbf{v}_l \neq 0$ is not a sufficient condition to guarantee the observability when bearing measurements are given in pseudo-linear format (see Appendix 1). However, it is the sufficient condition for system observability when consider the nonlinear bearing measurements in Cartesian coordinate system [36].

**Case 3:** Only range measurements are available

Bearing measurements are required in order to construct a pseudo-linear measurement model as expressed in Eq. 4. Hence, no pseudo-linear format exists for a range only exteroceptive sensory system. Thus, nonlinear range measurement has to employ with direct linearization for sensor fusion. Then the sufficient condition for the system to be locally weakly observable is 1) $\mathbf{v}_c \neq 0$ and 2) $\mathbf{v}_l \neq 0$ [36].

## 5 Simulation Results

The performance of the proposed relative localization scheme was evaluated in a series of numerical simulations. Each simulation was set up with a single leader robot and four child robots as illustrated in Fig. 2. 10 m × 20 m × 3 m 3D arena was selected as robots' navigation space.

For all simulation schemes, robot modeling inaccuracies and unmodelled internal and external disturbances are encapsulated within the low acceleration variance. The noise variances for relative range and bearing measurements are adapted from [13] and set to 0.007 m and 0.0036 rad, respectively. The frequency of the inter-robot relative observations is set to 10 Hz and the kinematic model is set to operate at 100 Hz. Twenty Monte Carlo simulation were performed and the results indicate the average values of all the variables.

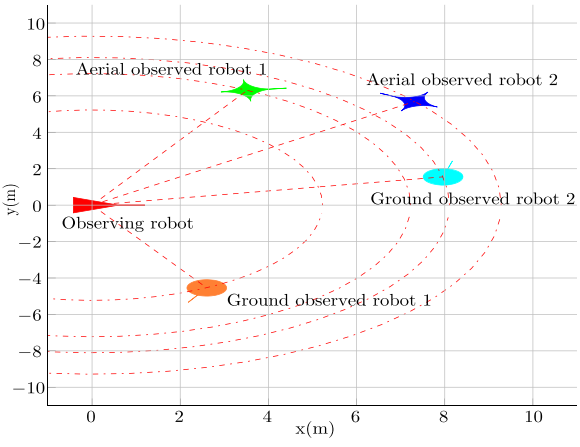


**Fig. 2** Simulation configuration

The initial simulation configuration assumed a team of mobile robots with the following characteristics; Total number of robots: 5; Number of observing robots: 1; Number of observed robots: 4. This simulation configuration is illustrated in Fig. 2. The navigation plane of the observing robot's sensor nodes is considered as the zero elevation level, and navigation planes for the first aerial, the second aerial, the first ground and the second ground observed robots were elevated to 2 m, 1.5 m, −0.1 m, and −0.2 m, respectively. Figure 3 illustrates the estimation errors and $3\sigma$ error boundaries for the first aerial observed robot. It can be seen that error is always within the $3\sigma$ error boundaries indicating that no overconfidence estimation occurs during the estimation process. This observation was identical for all other observed robots. Estimation errors for all four observed robots are depicted in Fig. 4 and demonstrate that the proposed RL scheme is capable of performing relative localization with 5∼10 cm positional accuracy and 0.075∼0.1 rad orientational accuracy.

### 5.1 Performance Comparison Against Traditional EKF Approach

The performance of the proposed method over a traditional EKF approach for arbitrary initialization is evaluated in the second simulation setup. This simulation configuration comprises an observing robot and an aerial observed robot. The navigation plane of the observed robot is elevated at 2 m above that of the observing robot's sensor nodes. All the presented results are the average of 20 Monte Carlo simulations. Four main cases are studied:

Case 1: The initial relative pose of the observed robot is accurately known.

Case 2: Only the initial relative position of the observed robot is known and the orientation is completely unknown.

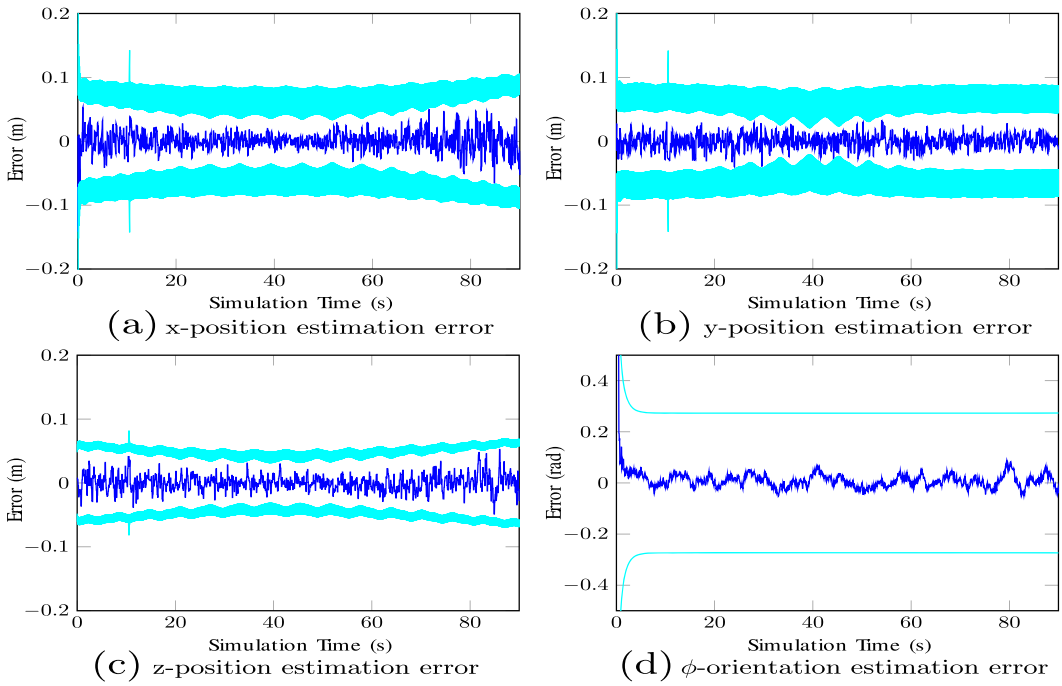


**Fig. 3** Average estimation error of aerial observed robot 1 for 20 Monte Carlo simulations. *Blue solid line* indicates error while *cyan solid lines* indicate double-sided $3\sigma$ error boundaries

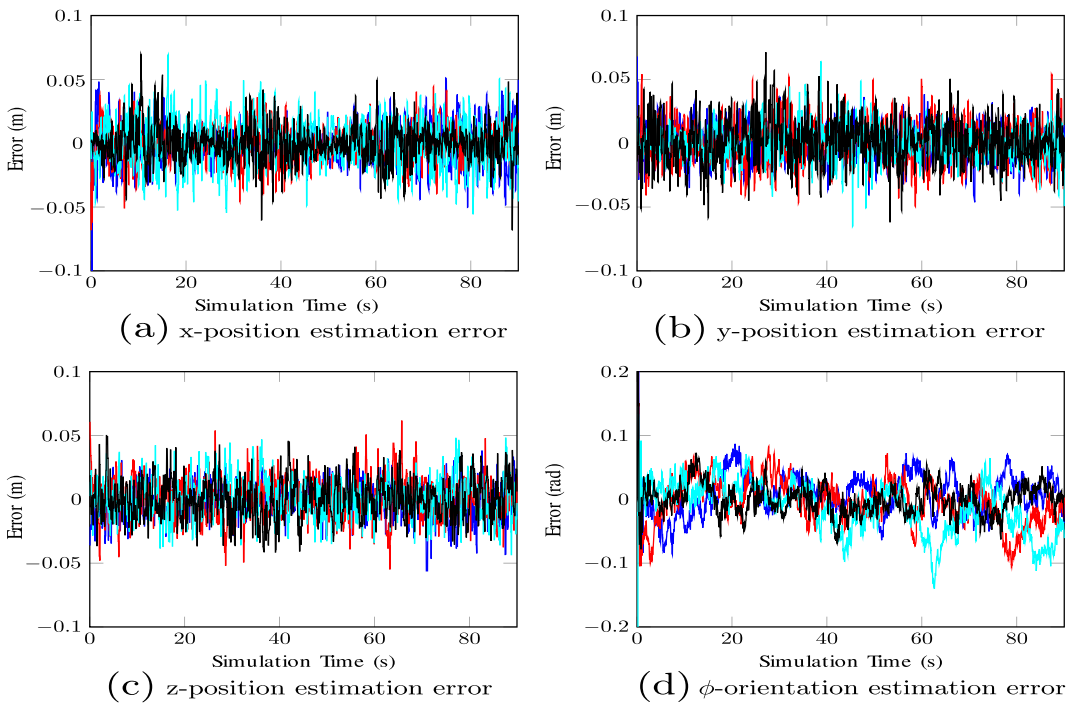


**Fig. 4** Average estimation error of all four observed robots for 20 Monte Carlo simulations. *Solid blue line*: aerial observed robot 1; *solid red line*: aerial observed robot 2; *solid cyan line*: ground observed robot 1; *solid black line*: ground observed robot 2

Case 3: The initial relative orientation of the observed robot is known and the initial relative position is set as random.

Case 4: The initial relative pose of the observed robot is completely unknown and set as random. In this case, 13 arbitrary initial poses have been simulated. These 13 arbitrary points are spatially distributed within the observing robot's field of view.

All the cases given above have been compared against the traditional EKF-based RL approach. For case 1, both the proposed method and traditional EKF approach exhibit similar performance in localization, where the initial relative pose is assumed to be known. The root mean squared errors (RMSE) of this case is shown in Fig. 5.

Maximum RMSE for each state estimation when relative localization is performed with known initial condition (i.e. maximum RMSE of case 1) is increased by 5 %, as defined in Eq. 32, and used as an upper bound for performance evaluation for arbitrary filter initializations.

$$\begin{aligned} x_{th} &\triangleq \max(X_{RMSE_{known\ initial\ pose}}) \times 1.05 \\ y_{th} &\triangleq \max(Y_{RMSE_{known\ initial\ pose}}) \times 1.05 \\ z_{th} &\triangleq \max(Z_{RMSE_{known\ initial\ pose}}) \times 1.05 \\ \phi_{th} &\triangleq \max(\phi_{RMSE_{known\ initial\ pose}}) \times 1.05 \end{aligned} \tag{32}$$

Figure 6 illustrates sample simulation outcomes for an arbitrary filter initialization, that was obtained in case 4. This result demonstrates that the proposed method outperforms for arbitrary filter initialization. Significant improvement could be achieved in relative orientation tracking.

Table 1 summarizes the number of measurement updates required for RL to converge to an acceptable accuracy level when the filter is initialized with arbitrary pose. Results presented for case 4 are the average result of 13 arbitrary initializations.

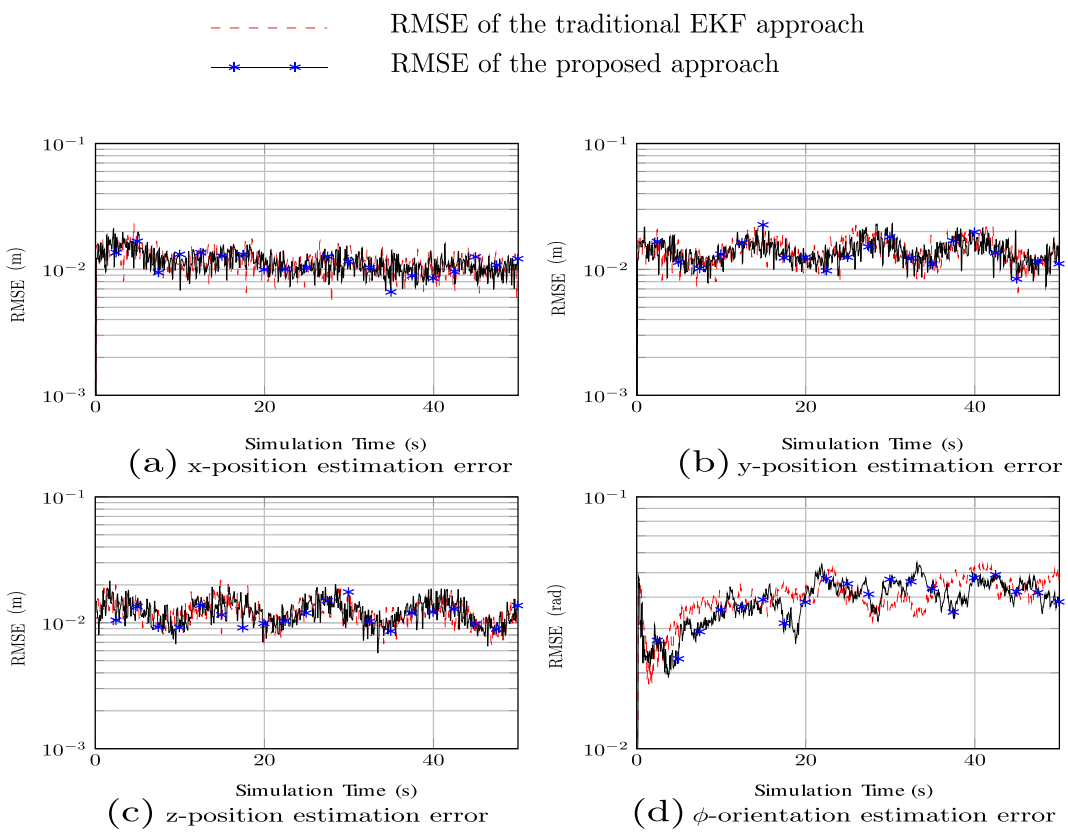


**Fig. 5** RMSE of relative pose measurement for case 1

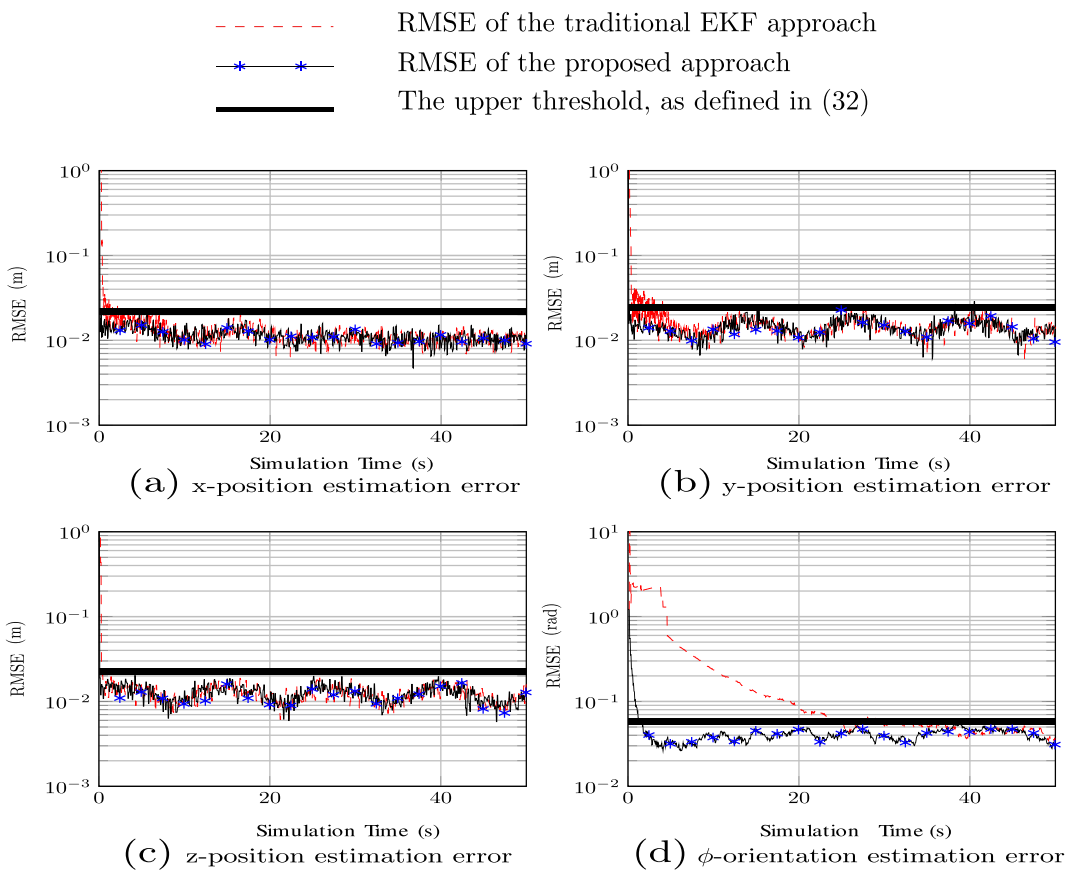


**Fig. 6** Comparison of the proposed method against the traditional EKF approach for arbitrary filter initialization

This results demonstrate that when the tracking is performed with arbitrary initialization, the proposed method is able to achieve both the positional and orientational accuracy within 12 iterations, whereas the traditional methods requires more than 250 iterations to achieve the same accuracy. As a result, settling

**Table 1** Number of measurement updates required for RL to converge to an acceptable accuracy level for the cases of inaccurate filter initialization [18]

| Relative state | Case 2 | | Case 3 | | Case 4 | |
|---|---|---|---|---|---|---|
| | PLKF[a] | TEKF[b] | PLKF | TEKF | PLKF | TEKF |
| $x$-position | 1 | 2 | 1 | 34 | 1 | 37 |
| $y$-position | 1 | 1 | 1 | 5 | 1 | 31 |
| $z$-position | 1 | 1 | 1 | 5 | 1 | 6 |
| $\phi$-orientation | 5 | 12 | 4 | 141 | 12 | 263 |

[a]PLKF: proposed pseudo-linear Kalman filter based approach.

[b]TEKF: traditional EKF approach

time of the RL is considerably smaller in the proposed method compared to the traditional EKF-based approach.

## 6 Experimental Results

An experimental validation of the proposed method for an unknown filter initialization was performed using a team of two Pioneer P3AT robots, as shown in Fig. 7. One Pioneer robot was treated as an observing robot while the other was treated as an observed robot. Both robots were provided with a map of the environment where the experiment was performed. The robots realized range and bearing for nearby static and dynamic objects using SICK LMS 200 laser scanners that were hosted on each robot. They then performed state-of-the-art map-based localization; this localization data served as the ground truth data for experimental evaluations.

### 6.1 Inter Robot Relative Measurements

Instead of implementing an exteroceptive sensory system that directly measures range and bearing for neighbouring robots, as presented in [13], we simulated the behaviour of an exteroceptive sensory system by analytically computing the relative range and bearing data from the ground truth data via Eq. 3, as suggested in [43]. This gave us the freedom to select the accuracy level of the exteroceptive sensory data and control its update rates. Such flexibility is required in order to evaluate the robustness of the proposed method for changing sensor noise levels and updating rates, as they are the parameters that potentially affect the estimation accuracy [20, 44]. Two measurement noise configurations and two update rates for exteroceptive sensory systems (as given in Table 2) were studied.

### 6.2 System Architecture

The system architecture of the experiment setup is illustrated in Fig. 8. Each robot acquired its egocentric (odometry) data and laser scan data. Scan matching-based localization is then performed by each robot. This localization data and odometry readings are then transmitted to a host computer through a TCP/IP interface. The ground truth data preparations; noisy relative range and bearing measurement construction; pseudo-linear measurement and corresponding measurement error variance matrix formation; and observed robot tracking were performed at the host computer. Estimated relative pose of the observed robot was then compared with the ground truth data. Note that the experiment setup was limited to 2D space; hence it was assumed that the observed robot's navigation plane was two metres above its actual navigation plane.

In regards to practical implementation, the observed robot may disappear from the field of view of the observing robot for few time steps due to the

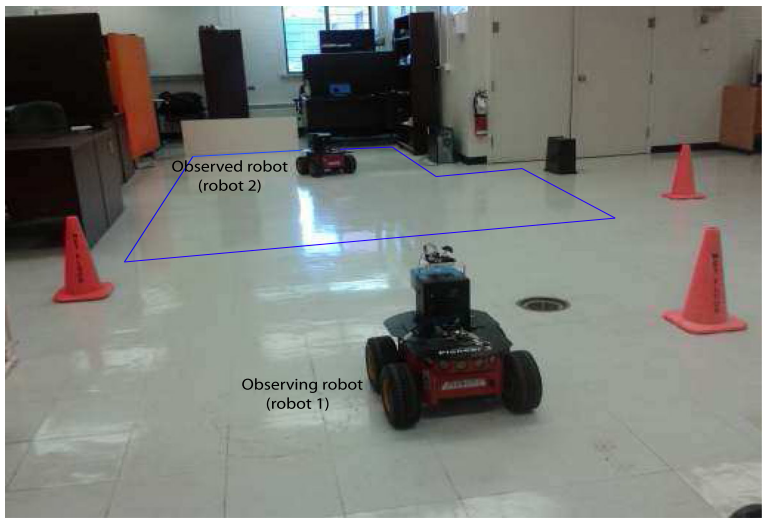


**Fig. 7** Experiment test bed which includes two pioneer P3AT robots

**Table 2** Characteristics of exteroceptive sensory systems

| Case | Noise levels for exteroceptive sensory system | Measurement update frequencies |
|---|---|---|
| **Case (1)** | $\sigma_r = 0.0068$m[a], $\sigma_\theta = 0.0036$ rad[b] [13][c] | 10 Hz |
| **Case (2)** | $\sigma_r = 0.1466$m, $\sigma_\theta = 0.1$ rad [45] | 10 Hz |
| **Case (3)** | $\sigma_r = 0.0068$m, $\sigma_\theta = 0.0036$ rad [13] | 1 Hz |
| **Case (4)** | $\sigma_r = 0.1466$m, $\sigma_\theta = 0.1$ rad [45] | 1 Hz |

[a]$\sigma_r$: standard deviation of the range measurements

[b]$\sigma_\theta$: standard deviation of the bearing measurements

[c]Note that [13] presents sensors' noise standard deviations in different units. Here we converted them into 'm' and 'rad' in order to facilitate comparison between two noise levels without undergoing any difficulties

static or dynamic obstacles in the navigation space. In such scenario, the deletion of the track corresponds to the observed robot may not be the best option. In fact, that track can be maintained for next few time steps and deleted if the observed robot does not reappear within the field of view of the observing robot within a pre-defined time window. If the observed robot reappears within the time window rapid convergence of relative pose estimation can be expected from the proposed relative localization scheme as now the observing robot has a partial knowledge about the relative pose of the observed robot. Note that once the track is deleted for the given observed robot and the same observed robot reappears within the field of view

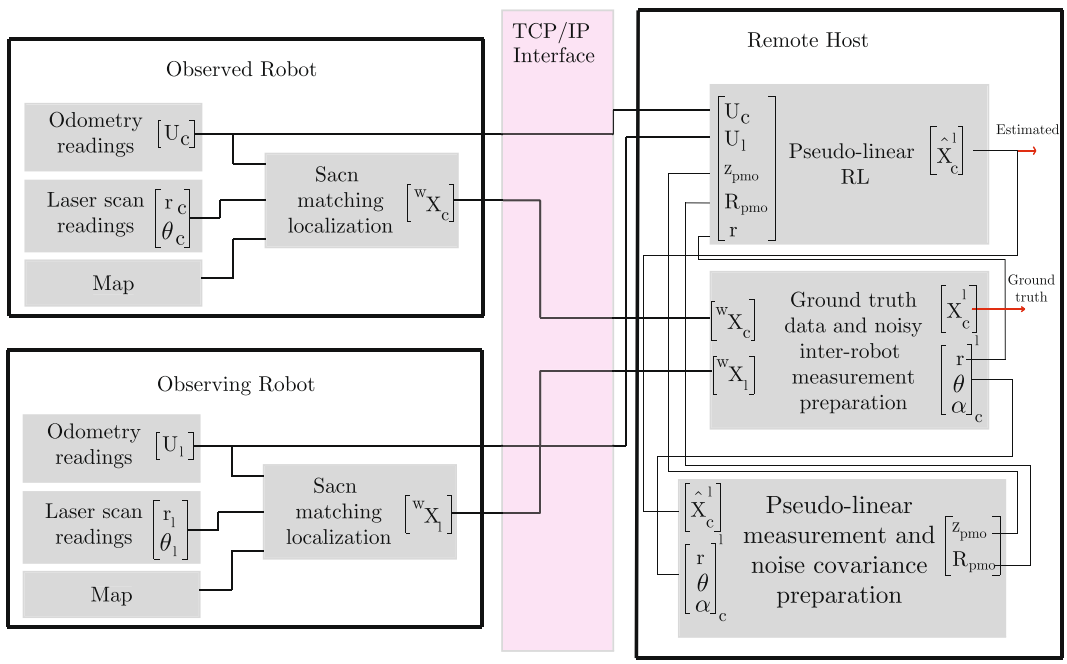


**Fig. 8** System architecture of the experiment setup to validate the proposed RL scheme

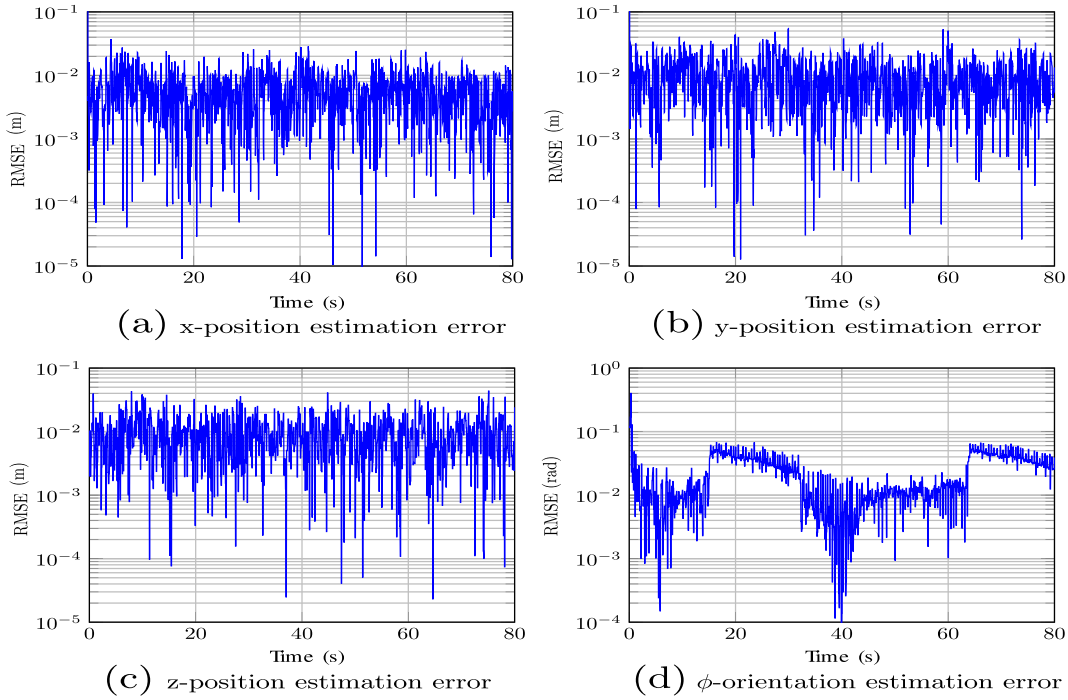


**Fig. 9** Relative localization accuracy of the proposed method for arbitrary filter initialization (Section 6)

of the observing robot, the observing robot initializes a new track. Current experiments have not evaluated this scenario and will be evaluated in the future work.

### 6.3 Results

Figure 9 illustrates RMSE of the observed robots pose estimation, for the noise level and update rate given in Case (1), using the proposed RL scheme when the filter was initialized with a completely unknown initial pose. The results are congruent with the simulation results, showing that the proposed method is capable of establishing the relative pose for observed robots with 5∼10 cm positional accuracy and 0.075∼0.1 rad orientational accuracy. Additionally, the proposed method demonstrates fast convergence property even though the filter is arbitrarilyinitialized.

Table 3 presents the comparison of the mean of the steady state RMSE and corresponding standard deviations (Std-RMSE) of the proposed relative localization scheme for all four scenarios given in Table 2. These results can be summarized as follows:

**Table 3** Comparison of relative pose estimation error for the observed robot at different IRRM update rates and different noise levels of exteroceptive sensory system

| | $\phi$-orientation estimation | | $x$-position estimation | | $y$-position estimation | | $z$-position estimation | |
|---|---|---|---|---|---|---|---|---|
| Case | RMSE (rad) | Std-RMSE (rad) | RMSE (m) | Std-RMSE (m) | RMSE (m) | Std-RMSE (m) | RMSE (m) | Std-RMSE (m) |
| Case (1) | 0.0313 | 0.0341 | 0.0098 | 0.0028 | 0.0131 | 0.0038 | 0.0123 | 0.0032 |
| Case (2) | 0.0962 | 0.0447 | 0.0925 | 0.0210 | 0.1264 | 0.0304 | 0.0849 | 0.0201 |
| Case (3) | 0.0443 | 0.0820 | 0.0266 | 0.0227 | 0.0357 | 0.0463 | 0.0135 | 0.0042 |
| Case (4) | 0.1836 | 0.1431 | 0.1510 | 0.0380 | 0.2246 | 0.0629 | 0.1439 | 0.0353 |

- The mean of the RMSE and corresponding standard deviations increased with the increases of the uncertainty of the exteroceptive sensory system.
- The mean of the RMSE and corresponding standard deviations increased with the decreases of the update rate of the exteroceptive sensory system.
- When an observing robot was equipped with a highly accurate sensory system (e.g. [13]), then the proposed relative localization scheme was capable of establishing relative localization with 0∼8 cm positional accuracy and 0∼0.13 rad orientational accuracy for both 10 Hz and 1 Hz exteroceptive measurement update rate.
- When the exteroceptive sensory system had high measurement uncertainty, then the proposed relative localization scheme was capable of establishing relative localization with 0∼16 cm positional accuracy and 0∼0.15 rad orientational accuracy for the 10 Hz exteroceptive measurement update rate, and with 0∼27 cm positional accuracy and 0∼0.33 rad orientational accuracy for the 1 Hz exteroceptive measurement update rate.

## 7 Consistency Analysis

### 7.1 Normalized Estimation Error Squared (NEES) Test

To assess the consistency of the proposed RL scheme, NEES is computed, as given in Eq. 33.

$$\epsilon_P(k) = [\mathbf{x}(k) - \hat{\mathbf{x}}(k)]^T \mathbf{P}^{-1}(k|k)[\mathbf{x}(k) - \hat{\mathbf{x}}(k)] \quad (33)$$

where $\mathbf{x}$ and $\hat{\mathbf{x}}$ are true and estimated states and $\mathbf{P}$ is the estimation error covariance. NEES ($\epsilon_P(k)$) is a scalar value and follows Chi-square distribution with $n_x$-DOF, where $n_x$ is the number of dimensions in the state vector. For the hypothesis $H_\circ$ filter is consistent for single run if:

$$\epsilon_P(k) \leq \chi^2_{n_x,\delta} \quad (34)$$

where $\delta$ is the significance level. 95 % acceptable region for 4-DOF $(x, y, z, \phi)$ is upper bounded by $\chi^2_{4,0.95}$, which is equal to 9.4877. Figure 10 presents the NEES test results for the Case (1) of Table 2.

Table 4 summarizes the results that obtained from the NEES analysis.

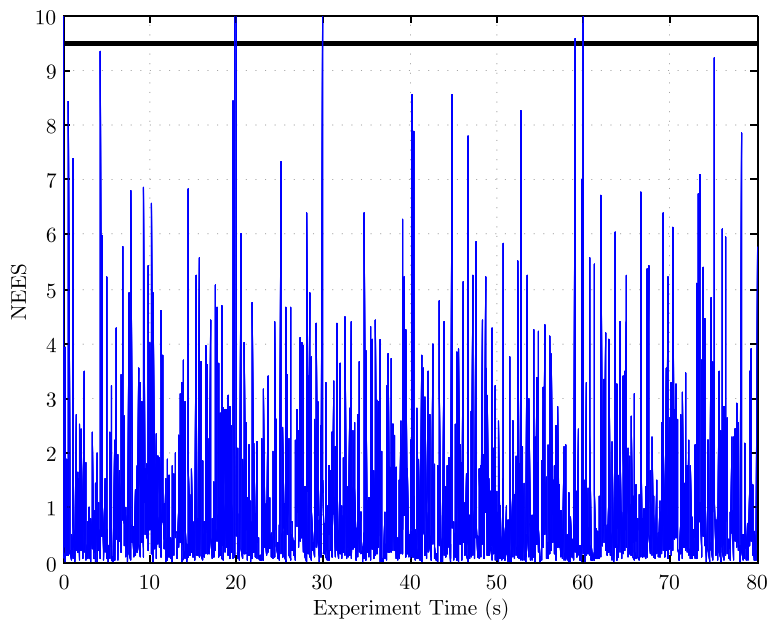


**Fig. 10** NEES values for the proposed method. Horizontal black line indicates the Chi-square upper bound

**Table 4** Percentage of NEES values that beyond the Chi-square upper bound ($\chi^2_{4,0.95} = 9.4877$)

| Case | % of NEES value that beyond the upper boundary |
|---|---|
| **Case (1)** | 0.0625 % |
| **Case (2)** | 2.9375 % |
| **Case (3)** | 4.6875 % |
| **Case (4)** | 9.25 % |

For the proposed method, less than 10 % of the values fall outside of the 95 % region, as listed in Table 4, which is acceptable [46, 47].

### 7.2 Normalized Innovation Squared (NIS) Test

The consistency of predicted measurements with actual measurements are evaluated using NIS as defined in Eq. 35.

$$\varepsilon_S(k) = \nu(k)^T \mathbf{S}(k)^{-1} \nu(k) \tag{35}$$

where $\mathbf{S}$ is the innovation covariance and $\nu$ is the innovation residual. $k$ is sample time step. NIS also follows Chi-squared distribution with $n_x$ degree of freedom where $n_x$ is the number of measurements. 95 % acceptable region for 3 degree of freedom ($y_1$, $y_2$, $y_3$ given in Eq. 3) is upper bounded by $\chi^2_{3,0.95}$ which is equal to 7.8147. Figure 11 presents the NIS test results for the Case (1) of Table 2.

It can be seen that all the NIS values are within the acceptable region. This observation was identical for all other scenarios given in Table 2. Hence, pseudo-linear measurements are consistent.

### 7.3 Covariance Conditioning

As measurements are transformed into pseudo-linear format the corresponding measurement covariances become a function of estimated states (Eq. 6). The error covariance $\mathbf{R}$ then becomes a time dependent compared to the constant measurement covariance in traditional EKF approaches. This dynamic nature may lead to ill-conditioning of the matrix $\mathbf{R}$; hence, the matrix $\mathbf{S}$ and the matrix $\mathbf{P}$. A covariance conditioning test, as proposed in [48], has been performed to evaluate the ill-conditioning nature of each covariance matrix. The condition value $C_{\mathbf{x}}$ for the given matrix is defined as Eq. 36.

$$C_{\mathbf{x}} = \log_{10}\left(\frac{\lambda_{max}}{\lambda_{min}}\right) \tag{36}$$

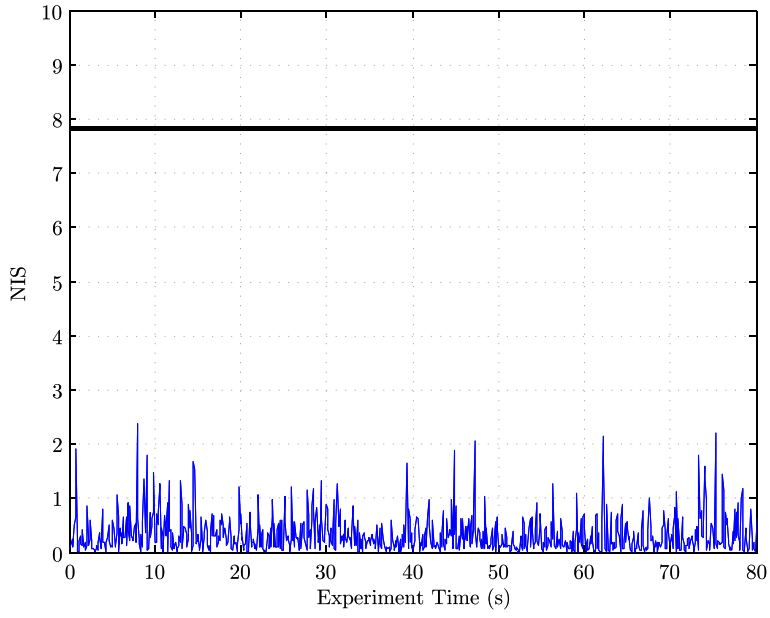


**Fig. 11** NIS values for the proposed method. Horizontal black line indicates the Chi-square upper bound

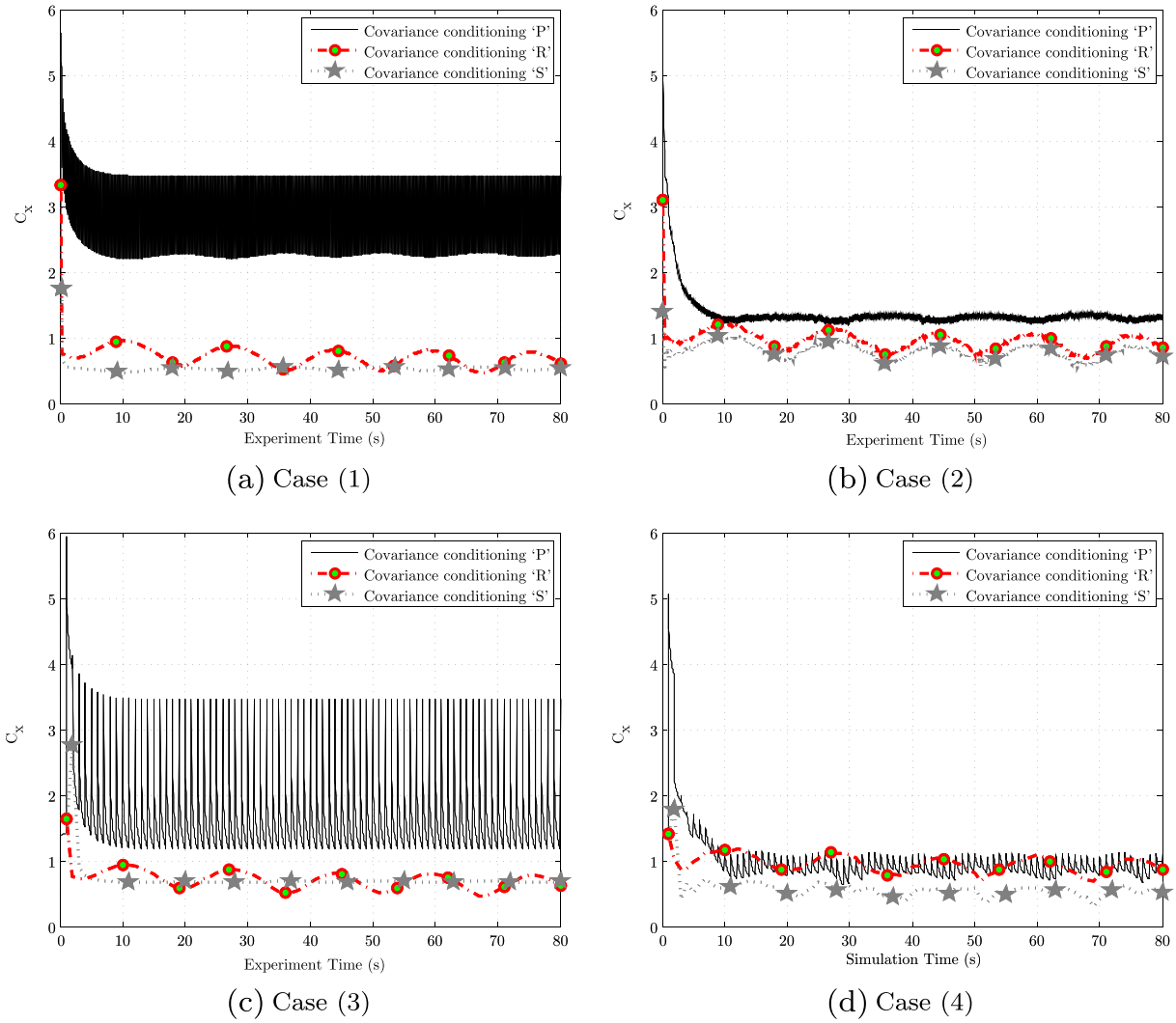


**Fig. 12** Covariance conditioning values for four test scenarios given in Table 2

where $\lambda_{min}$ and $\lambda_{max}$ are the minimum and the maximum eigenvalues of corresponding covariance matrices. The upper bound that represents good conditioning is set to 6, as given in [48]. Figure 12 illustrates that the covariance conditioning values for **P**, **R**, and **S** for all four test scenarios are below the conditioning bound ($C_{\mathbf{x}} = 6$), indicating that simplified, zero-mean temporally uncorrelated pseudo-measurement covariance matrix does not lead for ill-conditioning of any of the estimated covariances.

## 8 Conclusions and Future Works

This study applied pseudo-linear inter-robot relative measurement-based suboptimal filter for a relative localization. The proposed method was evaluated using an air-ground multi-robot system operating in an indoor environment. The results have demonstrated that the proposed method performs RL with 5∼10 cm positional accuracy and 0.075∼0.1 rad orientational accuracy. When the initial conditions are relaxed,

the pseudo-linear measurement-based approach has shown satisfactory accuracy. Additionally, it was more robust against unknown filter initialization and showed a faster convergence for an arbitrary filter initialization. This ability allowed an agent to disappear from an observing robots field of view and then reappear again in the system where they can be accurately localized when desired. The observability analysis showed that the proposed method can be applied for any relative localization application where the exteroceptive sensory system used for RL is capable of measuring relative bearing for neighbouring robots.

This work assumed that there is at least one robot available with sufficient computational and sensory capabilities to acquire the range and bearing information of multiple robots in an MRS. This work also assumed that the collaborative missions used both ground and aerial robots, where the less capable robots can be accurately manoeuvred using the sensors of the more capable robots. Additionally, this work assumed known data association for relative range and bearing measurements and obstacle free navigation space. Research is ongoing to integrate the state-of-the-art data association solution to the proposed RL scheme and integrate an exteroceptive sensory system that directly measures the relative range and bearing for neighbouring robots. This exteroceptive sensory system will be independent from the exteroceptive sensory system employed to get the ground truth data set. Additionally, obstacles will be added to the navigation space and evaluated the performance of track deletion and initialization process experimentally.

**Acknowledgments** The authors thankful to the Memorial University of Newfoundland and Natural Sciences and Engineering Research Council of Canada (NSERC) for their financial supports.

## Appendix 1

Consider an exteroceptive sensory system which is capable of measuring only the relative bearing for observed robots as given in Eq. 22. Furthermore, assume zeroth-order Lie derivatives (Eqs. 23 and 24) and first-order Lie derivatives (Eqs. 25 and 26) are available.

– Computes the first order Lie derivative $\mathfrak{L}^1_{\mathbf{f}_1}\mathbf{h}_2$

$$\mathfrak{L}^1_{f_1}\mathbf{h}_2 = \nabla\mathfrak{L}^{\circ}\mathbf{h}_2 \cdot \mathbf{f}_1 = \begin{bmatrix} s(\theta) & -c(\theta) & 0 \\ s(\alpha)c(\theta) & s(\alpha)s(\theta) & -c(\alpha) \end{bmatrix} \tag{37}$$

This is independent from the system states; thus, resulting gradient matrix is as follows:

$$\nabla\mathfrak{L}^1_{f_1}\mathbf{h}_2 = 0_{6\times 4} \tag{38}$$

New observability matrix then can be defined as Eq. 39.

$$\mathcal{O}_3 = \begin{bmatrix} \nabla\mathfrak{L}^{\circ}\mathbf{h}_2 \\ \nabla\mathfrak{L}^1_{\mathbf{f}_1}\mathbf{h}_2 \\ \nabla\mathfrak{L}^1_{\mathbf{f}_2}\mathbf{h}_2 \end{bmatrix} = \begin{bmatrix} \mathbf{h}^{\circ}_{pmo_2} & 0_{2\times 1} \\ 0_{6\times 3} & 0_{6\times 1} \\ 0_{6\times 3} & \nabla_{\phi}\mathfrak{L}^1_{\mathbf{f}_2}\mathbf{h}_2 \end{bmatrix} \tag{39}$$

Rank of the observability matrix $\mathcal{O}_3$ is three ($\text{rank}(\mathcal{O}_3) = 3$). This is less than the number of the state variables (DOF) in the state vector given in Eq. 1. Hence, $\mathbf{v}_c \neq 0$ and $\mathbf{v}_l \neq 0$ is not a sufficient condition to guarantee the observability when bearing measurements are given in pseudo-linear format.

## References

1. Hoffmann, G., Tomlin, C.: Decentralized cooperative collision avoidance for acceleration constrained vehicles. In: 47th IEEE Conference on Decision and Control. CDC, pp. 4357–4363 (2008)
2. Ikemoto, Y., Hasegawa, T.F., Matsuda, K.: Graduated spatial pattern formation of robot group. In: Information Science, vol. 171
3. Lee, G., Chong, N.Y.: Decentralized formation control for small-scale robot teams with anonymity. Mechatron. **19**(1), 85–105 (2009)
4. Kato, T., Watanabe, K., Maeyama, S.: A formation method for heterogeneous multiple robots by specifying the relative position of each robot. In: Proceedings of SICE Annual Conference 2010, pp. 3274–3277 (2010)
5. Shucker, B., Murphey, T., Bennett, J.K.: Convergence-preserving switching for topology-dependent decentralized systems. Robot. IEEE Trans. **24**(6), 1405–1415 (2008)
6. Antonelli, G., Arrichiello, F., Chiaverini, S.: Flocking for multi-robot systems via the null-space-based behavioral control. In: IEEE/RSJ International Conference on Intelligent Robots and Systems. IROS, pp. 1409–1414 (2008)
7. Pilz, U., Popov, A.P., Werner, H.: Robust controller design for formation flight of quad-rotor helicopters. In: CDC, 8322—8327 (2009)
8. Yang, M., Chu-yan, C., Tian, Y.-T.: A review of studies in flocking for multi-robot system. In: International

Conference on Computer, Mechatronics Control and Electronic Engineering (CMCE), vol. 4, pp. 28–31 (2010)
9. Stirling, T.S., Wischmann, S., Floreano, D.: Energy-efficient indoor search by swarms of simulated flying robots without global information. Swarm Intell. **4**(2), 117–143 (2010)
10. Howard, A., Mataric, M., Sukhatme, G.: Cooperative relative localization for mobile robot teams: an ego-centric approach. In: Naval Research Lab. Workshop on Multi-Robot Systems, pp. 65–76 (2003)
11. Rivard, F., Bisson, J., Michaud, F., Letourneau, D.: Ultrasonic relative positioning for multi-robot systems. In: IEEE International Conference on Robotics and Automation. ICRA, pp. 323–328 (2008)
12. Milella, A., Pont, F., Siegwart, R.: Model-based relative localization for cooperative robots using stereo vision. In: 12th annual Conference on Mechatronics and Machine Vision in Practice (2005)
13. De Silva, O., Mann, G., Gosine, R.: Development of a relative localization scheme for ground-aerial multi-robot systems. In: IEEE/RSJ International Conference on Intelligent Robots and Systems (IROS), pp. 870–875 (2012)
14. Martinelli, A., Pont, F., Siegwart, R.: Multi-robot localization using relative observations. In: Proceedings of the 2005 IEEE International Conference on Robotics and Automation, ICRA 2005, pp. 2797–2802 (2005)
15. Li, W., Zhang, T., Kuhnlenz, K.: A vision-guided autonomous quadrotor in an air-ground multi-robot system. In: IEEE International Conference on Robotics and Automation (ICRA), pp. 2980–2985 (2011)
16. Nettleton, E.W., Durrant-Whyte, H.F., Gibbens, P.W., Goektogan, A.H.: Multiple-platform localization and map building, vol. 4196 (2000)
17. Fenwick, J., Newman, P., Leonard, J.: Cooperative concurrent mapping and localization. In: Proceedings of IEEE International Conference on Robotics and Automation. ICRA '02, vol. 2, pp. 1810–1817 (2002)
18. Wanasinghe, T.R., Mann, G.K.I., Gosine, R.G.: Pseudo-linear measurement approach for heterogeneous multi-robot relative localization. In: IEEE 16th International Conference on Advanced Robotics (ICAR 2013) (Montevideo, Uruguay), November 2013 (to be published)
19. Carlone, L., Kaouk Ng, M., Du, J., Bona, B., Indri, M.: Simultaneous localization and mapping using rao-blackwellized particle filters in multi robot systems. J. Intell. Robot. Syst. **63**(2), 283–307 (2011)
20. Roumeliotis, S., Bekey, G.A.: Distributed multirobot localization. Robot. Autom. IEEE Trans. **18**(5), 781–795 (2002)
21. Bailey, T., Bryson, M., Mu, H., Vial, J., McCalman, L., Durrant-Whyte, H.: Decentralised cooperative localisation for heterogeneous teams of mobile robots. In: IEEE International Conference on Robotics and Automation (ICRA), pp. 2859–2865 (2011)
22. Xingxi, S., Tiesheng, W., Bo, H., Chunxia, Z.: Cooperative multi-robot localization based on distributed ukf. In: 3rd IEEE International Conference on Computer Science and Information Technology (ICCSIT), vol. 6, pp. 590–593 (2010)
23. Pathiranage, C., Watanabe, K., Jayasekara, B., Izumi, K.: Simultaneous localization and mapping: A pseudolinear kalman filter (PLKF) approach. In: 4th International Conference on Information and Automation for Sustainability. ICIAFS, pp. 61–66 (2008)
24. Guerra, E., Bolea, Y., Grau, A.: Pseudo-measured lpv kalman filter for slam. In: 10th IEEE International Conference on Industrial Informatics (INDIN), pp. 700–705 (2012)
25. Whitcombe, W.D.: Pseudo state measurements applied to recursive nonlinear ltering,: in In: Proceedings of the 3rd Symp. nonlinear estimation theory and its application, (San Diego, CA,) pp. 278–281 (1972)
26. Prorok, A., Bahr, A., Martinoli, A.: Low-cost collaborative localization for large-scale multi-robot systems. In: IEEE International Conference on Robotics and Automation. (ICRA), pp. 4236–4241 (2012)
27. Heng, L., Meier, L., Tanskanen, P., Fraundorfer, F., Pollefeys, M.: Autonomous obstacle avoidance and maneuvering on a vision-guided mav using on-board processing. In: IEEE International Conference on Robotics and Automation. (ICRA), pp. 2472–2477 (2011)
28. Lin, Y., Vernaza, P., Ham, J., Lee, D.: Cooperative relative robot localization with audible acoustic sensing. In: IEEE/RSJ International Conference on Intelligent Robots and Systems. (IROS), pp. 3764–3769 (2005)
29. Rivard, F., Bisson, J., Michaud, F., Letourneau, D.: Ultrasonic relative positioning for multi-robot systems. In: IEEE International Conference on Robotics and Automation. ICRA, pp. 323–328 (2008)
30. Franchi, A., Oriolo, G., Stegagno, P.: Mutual localization in a multi-robot system with anonymous relative position measures. In: IEEE/RSJ International Conference on Intelligent Robots and Systems. IROS, pp. 3974–3980 (2009)
31. Kapse, A., Gu, D., Hu, Z.: Using cricket sensor nodes for pioneer robot localization. In: International Conference on Mechatronics and Automation. ICMA, pp. 2008–2013 (2009)
32. Maybeck, P.S.: Stochastic models, estimation and control, vol. 1 (1979)
33. Rugh, W.J.: Linear system theory. Upper Saddle River, N.J.: Prentice Hall, 2nd ed (1996)
34. Sharma, R., Beard, R., Taylor, C., Quebe, S.: Graph-based observability analysis of bearing-only cooperative localization. Robot. IEEE Trans. **28**(2), 522–529 (2012)
35. Sharma, R., Quebe, S., Beard, R., Taylor, C.: Bearing-only cooperative localization. J. Intell. Robot. Sys. **72**(3–4), 429–440 (2013)
36. Trawny, N., Zhou, X., Zhou, K., Roumeliotis, S.: Interrobot transformations in 3-D. Robot. IEEE Trans. **26**(2), 226–243 (2010)
37. Martinelli, A., Siegwart, R.: Observability analysis for mobile robot localization. In: IEEE/RSJ International Conference on Intelligent Robots and Systems. (IROS), pp. 1471–1476 (2005)
38. Kassas, Z.M., Humphreys, T.E.: Observability analysis of opportunistic navigation with pseudorange measurements. In: Proceedings of AIAA Guidance, Navigation

and Control Conference (GNC 12), pp. 4760–4775 (2012)
39. Hermann, R., Krener, A.J.: Nonlinear controllability and observability. IEEE Trans. Autom. Control **22**(5), 728–740 (1977)
40. Pathiranage, C., Watanabe, K., Izumi, K.: Simultaneous localization and mapping (slam) based on pseudolinear measurement model with a bias reduction approach. In: International Conference on Industrial and Information Systems. ICIIS, pp. 73–78 (2007)
41. Speyer, J.T., Song L.: A comparison between the pseudomeasurement and extended kalman observers. In: 20th IEEE Conference on Decision and Control including the Symposium on Adaptive Processes, vol. 20, pp. 324–329 (1981)
42. Song, T., Ahn, J., Park, C.: Suboptimal filter design with pseudomeasurements for target tracking, IEEE Trans. Aerosp. Electron. Syst. **24**(1), 28–39 (1988)
43. Cognetti, M., Stegagno, P., Franchi, A., Oriolo, G., Bulthoff, H.: 3-d mutual localization with anonymous bearing measurements. In: IEEE International Conference on Robotics and Automation (ICRA), pp. 791–798 (2012)
44. Song, Y., Li, Q., Kang Y., Song, Y.: Cfastslam: A new jacobian free solution to slam problem. In: IEEE International Conference on Robotics and Automation (ICRA), pp. 3063–3068 (2012)
45. Leung, K.Y.K.: Cooperative localization and mapping in sparsely-communicating robot network. University of Toronto, Phd. thesis (2012)
46. Bar-Shalom, Y., Kirubarajan, T., Li, X.-R.: Estimation with Applications to Tracking and Navigation. New York, NY, USA: John Wiley (2002)
47. Bahr, A., Walter, M., Leonard, J.: Consistent cooperative localization. In: IEEE International Conference on Robotics and Automation. ICRA '09, pp. 3415–3422 (2009)
48. Simpson, R., Revell, J.: Towards a taxonomy of performance metrics, bounds and tests for tracking and slam algorithms. In: SEAS DTC Technical Conference, 2009 (2009)